Scilight

Nano-electrochemistry & Nano-photochemistry
https://www.sciltp.com/journals/nenp

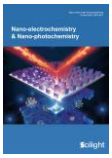

Review

In-Situ/Operando Raman Spectroscopy Techniques for In-Depth Decoupling CO_2 Reduction Reaction Mechanisms

Jinxia Xue, Ruixin Yang and Zixuan Chen *

State Key Laboratory of Analytical Chemistry for Life Science, School of Chemistry and Chemical Engineering, Nanjing University, Nanjing 210023, China
* Correspondence: chenzixuan@nju.edu.cn

How To Cite: Xue, J.; Yang, R.; Chen, Z. *In-Situ/Operando* Raman Spectroscopy Techniques for in-Depth Decoupling CO_2 Reduction Reaction Mechanisms. *Nano-electrochemistry & Nano-photochemistry* **2025**, *1*(1), 2. https://doi.org/10.53941/nenp.2025.100002.

Received: 28 September 2025
Revised: 16 October 2025
Accepted: 17 October 2025
Published: 27 October 2025

Abstract: Electrocatalytic carbon dioxide reduction reaction (eCO_2RR) is a pivotal negative carbon technology that converts greenhouse gas CO_2 into value-added chemicals using renewable energy. However, its selectivity and efficiency are still limited by an incomplete understanding of active-phase dynamics, key intermediate formation, and reaction-pathway identification. Due to its molecular-level structural sensitivity and real-time monitoring capability, *in-situ* Raman spectroscopy has become a powerful tool for decoupling eCO_2RR mechanisms by providing surface/interface-specific molecular fingerprints. This minireview systematically classifies and summarizes recent advances of *in-situ* Raman techniques applied to eCO_2RR, emphasizing the enhancement principles and design strategies of each technique. The discussed approaches include surface-enhanced Raman spectroscopy, shell-isolated nanoparticle-enhanced Raman spectroscopy, nanoconfinement-enhanced Raman spectroscopy, membrane electrode assembly-based Raman spectroscopy, and sub-second time-resolved surface-enhanced Raman spectroscopy. Representative examples highlight how these techniques decouple complex mechanisms, from active-phase evolution to intermediate identification and pathway elucidation. Furthermore, we provided a mechanism map linking Raman-observable intermediates to elementary reaction steps, highlighted recent innovations in Raman cell design, and discussed future directions toward multimodal integration and quantitative analysis. This focused and critical perspective provides a practical roadmap for researchers aiming to apply *in-situ* Raman spectroscopy in complex electrocatalytic systems.

Keywords: *in-situ* Raman spectroscopy; electrocatalytic carbon dioxide reduction reaction; reaction mechanism; reaction intermediate; Raman cell innovations

1. Introduction

To tackle severe climate change and energy crisis, the development of efficient carbon-neutral technologies has become a key strategy for global sustainable development [1,2]. The electrocatalytic carbon dioxide reduction reaction (eCO_2RR) uses renewable electricity, converting greenhouse gas CO_2 into value-added chemicals [3,4]. However, the CO_2 molecule is extremely stable in thermodynamic facet, and its linear structure possesses a dissociation energy of the C=O bond as high as 750 $kJ \cdot mol^{-1}$, making its activation and subsequent conversion challenging [5]. Moreover, eCO_2RR involves complex multi-electron transfer pathways and competes with the hydrogen evolution reaction, both of which severely limit reaction efficiency and kinetics [6,7]. Therefore, deeply understanding the dynamic evolution of catalyst active phases and identifying key adsorbed intermediates, and elucidating reaction pathways are essential to overcome current bottlenecks [8,9]. During the eCO_2RR process, low-concentration and short-lived intermediates at the three-phase dynamic interface are highly sensitive to the

local electric field and electrolyte environment [10]. Traditional *ex-situ* characterizations generally difficult to capture these intermediates in realistic reaction conditions.

To address these challenges, diverse *in-situ* characterization techniques have been developed in recent years. For instance, transmission electron microscopy, X-ray diffraction, and X-ray absorption spectroscopy (XAS) have been proven invaluable for capturing the dynamic evolution of crystal structures, crystalline defects, and chemical coordination environments [11–13]. Similarly, X-ray photoelectron spectroscopy can provide critical information about surface morphology and chemical state [14]. Vibrational spectroscopies, especially *in-situ* Raman spectroscopy and infrared spectroscopy, can reveal surface/interface dynamics and reaction pathways at the molecular level [15,16]. Among them, the *in-situ* Raman spectroscopy is sensitive to low-frequency modes and can deliver structural fingerprints of molecules and intermediates through vibrational modes. Moreover, due to the inherently small Raman cross-section of H_2O, it minimizes interference from water [17,18]. These characteristics enable direct probe of the three-phase reaction layer under realistic operating conditions. Nonetheless, the intrinsically low scattering efficiency of Raman spectroscopy results in a weak signal; thus, enhancing sensitivity remains a pivotal target. In addition, conventional *in-situ* Raman techniques suffer from strong background interference and limited spatiotemporal resolution in the complex electrochemical environments of eCO_2RR, hindering the accurate detection of transient intermediates and nanoscale active sites. To overcome these limitations, surface-enhanced Raman spectroscopy (SERS) has been widely applied to eCO_2RR. Contributing to localized surface plasmon resonance (LSPR) on nanostructured Au, Ag, or Cu substrates, SERS generates an intense local electromagnetic field that amplifies the Raman scattering of adsorbed molecules by 10^4–10^6 folds or more [19,20]. Based on it, various advanced SERS-based *in-situ* techniques have recently been developed for eCO_2RR studies, including shell-isolated nanoparticle-enhanced Raman spectroscopy (SHINERS) [21,22], nanoconfinement-enhanced Raman spectroscopy (NCERS) [23,24], membrane electrode assembly (MEA) -based Raman spectroscopy [25,26], and sub-second time-resolved SERS (STR-SERS) [27].

Although several reviews have discussed the application of *in-situ* Raman techniques in eCO_2RR, most of them either provide general overviews of Raman techniques or focus on a single enhancement strategy [19,28–32]. This minireview offers a systematic, comparative analysis of five *in-situ* Raman techniques specifically applied to eCO_2RR. We not only summarized their enhancement principles and design strategies but also provided a mechanism map linking Raman-observable intermediates to elementary reaction steps. Furthermore, we highlighted recent innovations in Raman cell design and discussed future directions toward multimodal integration and quantitative analysis. This focused and critical perspective differentiates our work from previous reviews and provides a practical roadmap for researchers aiming to apply *in-situ* Raman spectroscopy in complex electrocatalytic systems.

2. Working Principle of SERS

SERS, as a sensitivity vibrational spectroscopy technique, significantly amplifies intrinsic Raman signals of molecules adsorbed on or near coinage-metal surfaces with an enhancement factor of 10^4–10^6 folds or even higher [33–35]. Therefore, SERS has become a powerful tool for surface/interface research, single-molecule detection, and *operando* electrochemistry. As illustrated in Figure 1, the signal enhancement of SERS originates from two synergistic mechanisms, including electromagnetic enhancement (EM) and chemical enhancement (CE) [36]. The EM enhancement principle arises from the collective oscillation of free-electron clouds in nanostructured Au, Ag, or Cu substrates under laser excitation. This process generates an intense evanescent field, thus amplifying the Raman scattering from molecules within the field. CE arises from electronic coupling at the adsorbate-metal interface, which alters the molecular polarizability and consequently enhances the Raman scattering cross-section. As EM contributes the dominant factor (10^4–10^6 folds), typically exceeding CE (10–100 folds) [37,38], SERS activity is principally governed by the morphology and dielectric environment of the plasmonic nanostructure.

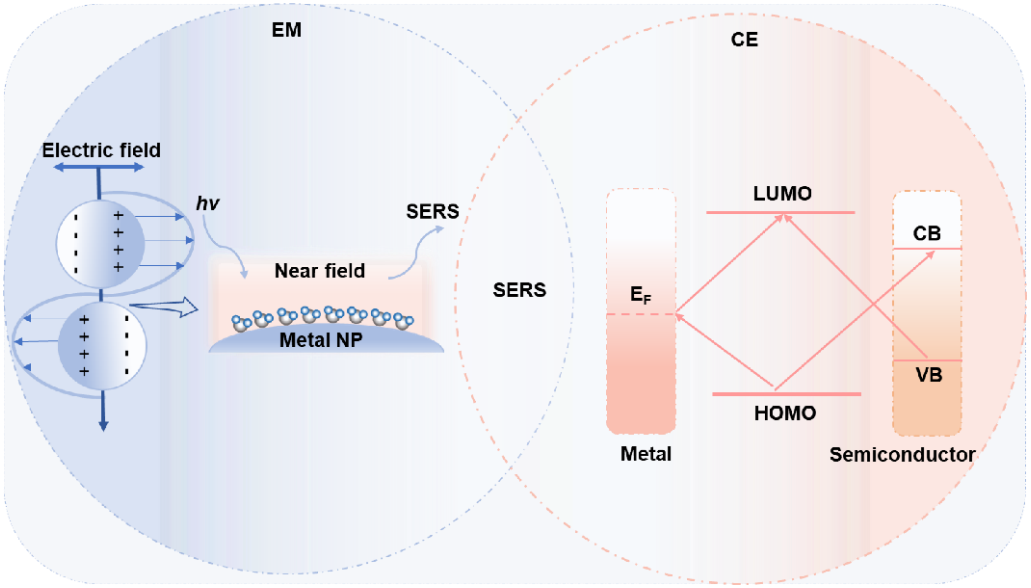

Figure 1. Schematic illustration of the EM and CM mechanisms in SERS. The EM mechanism arises from LSPR on nanostructured Au, Ag, or Cu surfaces, generating intense electromagnetic fields that amplify Raman signals by factors of 10^4–10^6. The CM mechanism involves charge transfer between adsorbates and the metal surface, enhancing the molecular polarizability. These synergistic mechanisms enable sensitive detection of intermediates and real-time monitoring of dynamic processes at electrocatalytic interfaces, providing key insights into reaction pathways and active-site behaviors in eCO_2RR. EM, electromagnetic enhancement; CM, chemical enhancement; SERS, surface-enhanced Raman spectroscopy; LSPR, localized surface plasmon resonance; eCO_2RR, electrocatalytic carbon dioxide reduction reaction.

3. *In-Situ* Raman Spectroscopy Techniques

The rapid evolution of SERS-based spectroscopy techniques has equipped researchers with increasingly powerful tools to decouple the complex mechanisms of eCO_2RR. These techniques are developed for overcoming the intrinsic challenges from weak Raman scattering, short-lived intermediates, and complex catalytic environments by tailoring enhancement strategies. To provide a concise strategic overview for readers, Table 1 compares the principal advantages, inherent limitations, and representative applications of regular SERS, SHINERS, NCERS, MEA-based Raman spectroscopy, and STR-SERS in eCO_2RR.

Table 1. Comparative summary of *in-situ*/*operando* Raman spectroscopy techniques applied to eCO_2RR.

Techniques	Advantages	Limitations	Representative Applications in eCO_2RR
Regular SERS [39,40]	Simple setup	Limited spatial resolution (~500 nm); strong background interference; restricted to roughened substrates	Tracking dynamic Cu oxide reduction/oxidation
SHINERS [21,22,36,41]	Non-invasiveness; applicable to single-crystal and flat surfaces; low background interference	Thick shell-limited enhancement; complex synthesis	Intermediate identification on a different single-crystal Cu surface
NCERS [23,24]	Ultra-high sensitivity; high spatiotemporal resolution; single site-based detection	Fabrication challenge; limited specific nanostructure	High spatiotemporally resolved C-C coupling pathways in Au@Cu nanogaps
MEA-based Raman spectroscopy [25,26,42–44]	Compatible with high current density, zero-gap structure, and polymer electrolyte interface; coupling with MS	Limited spatial resolution; measurement errors resulting from non-uniform current/potential distributions; restricted optical access	Detection of *CCO intermediate under high current density
STR-SERS [27,45]	Sub-second temporal resolution; tracking fast interfacial reactions	Dependence on *in-situ* construction of SERS hotspots	Low-frequency *CO linked to C_2H_4 formation

Note: SERS, surface-enhanced Raman spectroscopy; SHINERS, shell-isolated nanoparticle-enhanced Raman spectroscopy; NCERS, nanoconfinement-enhanced Raman spectroscopy; MEA, membrane electrode assembly; STR, sub-second time-resolved; MS, mass spectrometry.

3.1. Regular SERS

The SERS enhancement effect is strongly governed by the surface morphology of the substrate, where nanoscale roughness contributes to remarkable signal amplification [46]. Based on it, regular SERS has delivered valuable mechanistic insight into eCO_2RR. Cu-based catalysts possess a unique ability to produce multi-carbon products in eCO_2RR. Particularly, oxide-derived Cu (OD-Cu) catalysts are interesting, because their activity toward C_{2+} products is closely linked to reversible Cu^0/Cu^I redox cycling [39]. Yang et al. employed *in-situ* SERS to follow the dynamic evolution of active phases and key species on the surface of Cu foam in CO_2-saturated 0.1 M $KHCO_3$ [40]. In Figure 2A, at −0.2 V (vs. Ag/AgCl), broad bands corresponding to Cu oxides/hydroxides (Cu_xOH_y) are observed at 525 cm^{-1} and 620 cm^{-1}. These bands undergo a red shift within a short period of 3 s. Subsequently, the bands disappear completely within 12 s, leading to the formation of an active metallic Cu layer. This transformation coincides with the emergence of carbonate (1068 cm^{-1}) and linearly adsorbed CO (2107 cm^{-1}). Thus, the rapid reduction of surface oxides enables the real-time construction of a Cu active substrate. In Figure 2B, at +0.6 V, the pre-reduced Cu is re-oxidized to Cu_xOH_y within 12 s, with the appearance of a new atop CO peak (2148 cm^{-1}). These data provide direct evidence for rapid redox-mediated activation of OD-Cu foams and reveal potential-dependent CO adsorption geometries relevant to C-C coupling selectivity.

Similarly, *in-situ* Raman techniques have been applied to non-Cu catalyst systems like Bi or Pd, which are selective for HCOOH or CO production. For instance, for Bi-based catalysts (e.g., $Bi@Bi_2O_3$), *in-situ* Raman spectroscopy identified the *OCHO intermediate at 1469 cm^{-1} under reduction potentials, which was key for the HCOOH-selective pathway [47]. For Pd-based catalysts like PdNi alloys, Raman spectroscopy detected *COOH-related peaks at 1064 cm^{-1}, elucidating the CO-selective pathway with enhanced activity [48]. These examples demonstrate that Raman spectroscopy techniques can capture intermediate dynamics and reaction mechanisms in diverse catalyst systems, broadening the applicability beyond Cu-dominated studies. Despite these applications, regular SERS suffers from several inherent limitations, such as the optical diffraction limit (~500 nm) and strong background interference, which could obscure nanoscale heterogeneity and low-frequency modes.

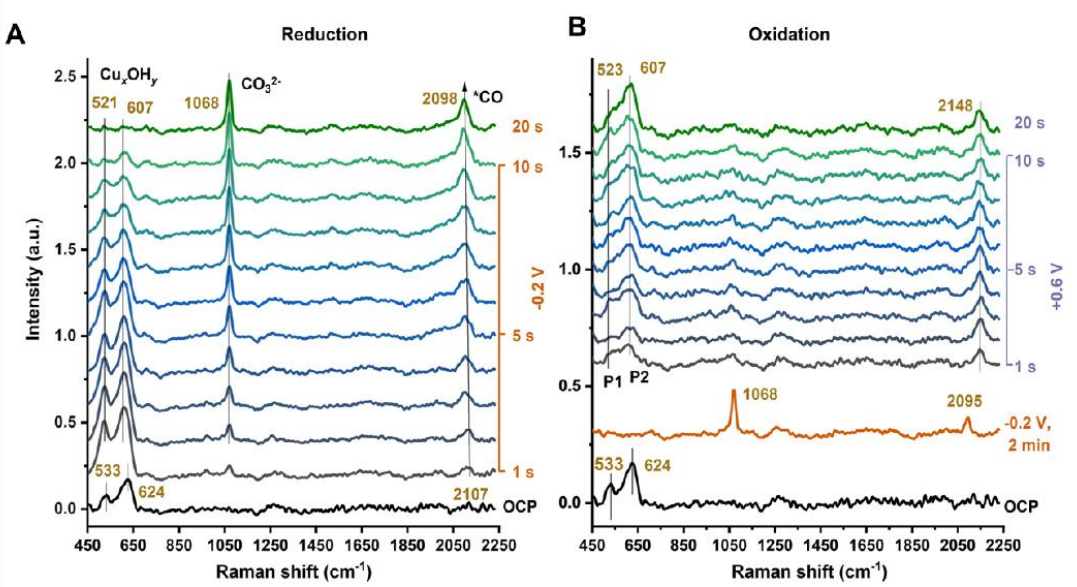

Figure 2. Tracking dynamic active-phase evolution on Cu foam during eCO_2RR using regular SERS. *Operando* SERS spectra recorded on Cu foam in CO_2-saturated 0.1 M $KHCO_3$ (pH 6.8). (**A**) Reduction at −0.2 V and (**B**) Re-oxidation at +0.6 V. Adapted from Ref. [40] with permission. Copyright 2024, Springer Nature. eCO_2RR, electrocatalytic carbon dioxide reduction reaction; SERS, surface-enhanced Raman spectroscopy.

3.2. SHINERS

Single-crystal electrode is regarded as a key model for obtaining deep insights into reaction mechanisms in eCO_2RR; regular SERS is restricted to roughened or nanostructured polycrystalline surfaces. SHINERS overcomes this limitation by introducing an ultrathin and chemically inert spacer between the plasmonic core and the electrode. Typically, 55–120 nm Au or Ag nanocrystals are coated with 2–5 nm of SiO_2 or Al_2O_3 shell. The dielectric shell is thin enough to allow the generated LSPR field to penetrate, delivering signal enhancement of 10^6–10^7 folds. Meanwhile, it prevents direct contact of the plasmonic core and the electrocatalytic environment, avoiding the occurrence of side reactions. Therefore, SHINERS can be deployed on atomically flat single crystals,

oxide films, or even polymer membranes, significantly broadening the types of catalytic systems compatible with *operando* Raman spectroscopy [49,50]. Recently, to probe the actual states of catalyst surface species in the reaction process, Zhao et al. pioneered the use of *in-situ* SHINERS to systematically research the surface-adsorbed species [21]. Specifically, as shown in Figure 3A, B, this study focused on the changes in surface-adsorbed species on different Cu surfaces, including Cu foil and Cu micro/nanoparticles under negative potentials in alkaline electrolytes. At −0.6 V vs. RHE, distinct behaviors were observed on different electrode surfaces. CuO_x-related bands (300 cm^{-1}, 540 cm^{-1}) exhibit prolonged stability on the smooth foil. $CuO_x/(OH)_y$ species accumulate preferentially on the micro-rough substrate. Moreover, the amount of these surface oxygen-containing species doesn't correlate positively with C_{2+} Faradaic efficiency. It implied that subsurface oxide rather than surface oxide modulates C-C coupling. This work not only exhibited the non-invasive enhancement advantage of SHINERS for electrocatalyst interfaces, but also provided a solid foundation for the study of the structure-activity relationship of Cu-based catalysts.

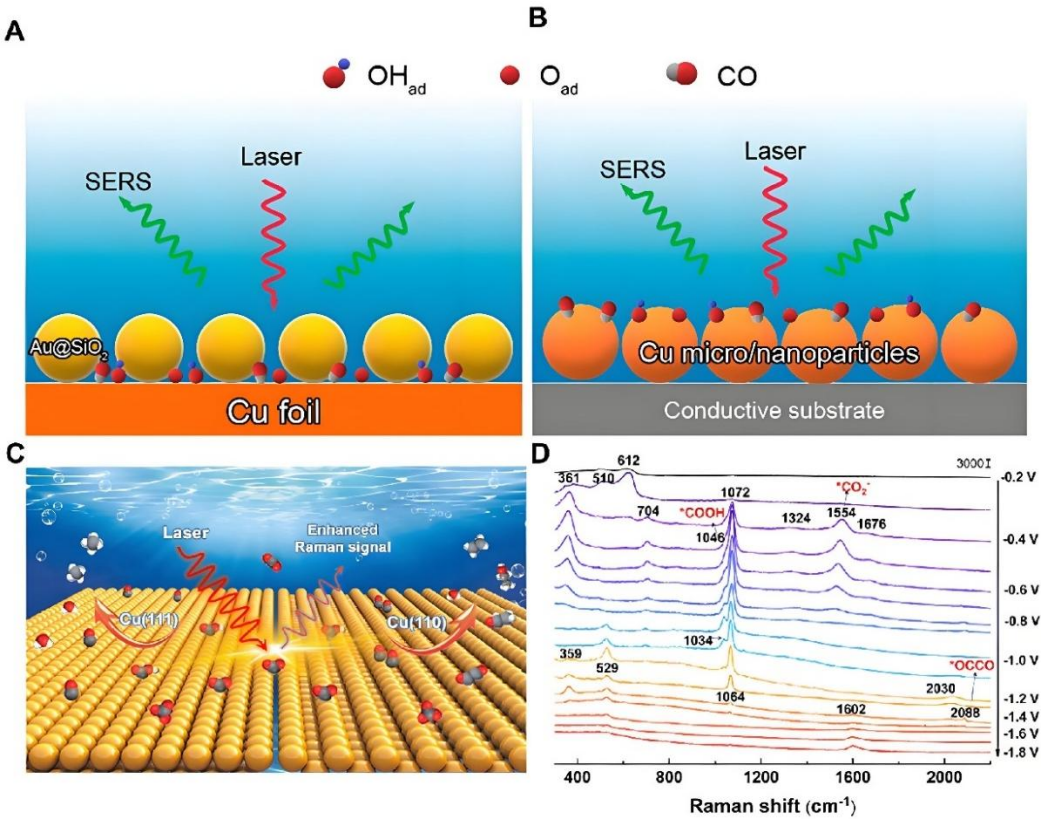

Figure 3. Probing facet-dependent intermediate speciation on single-crystal Cu surfaces during eCO_2RR using SHINERS. Schematic illustration of adsorbed species on Cu foil (**A**) and Cu micro/nanoparticles (**B**) surfaces under negative potentials in alkaline electrolytes. Adapted from Ref. [21] with permission. Copyright 2020, American Chemical Society. (**C**) Schematic illustration of intermediate species in eCO_2RR on Cu(111) and Cu(110) single-crystal surfaces through *in-situ* Raman spectroscopy. (**D**) *In-situ* Raman spectra of Cu(110) in a CO_2-saturated 0.5 M $KHCO_3/H_2O$ solution at various potentials (vs. SCE). Adapted from Ref. [22] with permission. Copyright 2022, The Royal Society of Chemistry. eCO_2RR, electrocatalytic carbon dioxide reduction reaction; SHINERS, shell-isolated nanoparticle-enhanced Raman spectroscopy; SCE, saturated calomel electrode.

Similarly, in Figure 3C, Li et al. performed facet-resolved SHINERS on Cu(111) and Cu(110) single-crystal electrodes [22]. By sweeping the potential from −0.2 V to −1.0 V vs. SCE in CO_2-saturated 0.5 M $KHCO_3$, they identified $*CO_2^-$ (361 cm^{-1}, 704 cm^{-1}, 1324 cm^{-1}, 1554 cm^{-1}), *COOH (1046 cm^{-1}), *CO (2030–2088 cm^{-1}), *OCCO (2088 cm^{-1}), and $*CH_2CHO$ (529 cm^{-1}). As presented in Figure 3D, potential-dependent Raman spectroscopy revealed that the Cu(110) surface produced C_2 products via the $*OCCO \rightarrow *CH_2CHO$ pathway, while Cu(111) mainly generated C_1 products through the $*COOH \rightarrow *CO$ pathway. Raman spectroscopy also demonstrated that high-concentration $KHCO_3$ can enhance *CO coverage and promote C-C coupling, underscoring the dual control offered by surface atom arrangement and local electrolyte concentration. Thus, these studies suggest SHINERS can be a versatile tool for probing well-defined electrocatalysts under realistic conditions, and bridge the gap between single-crystal model systems and practical nanomaterials.

3.3. NCERS

Although SHINERS extends SERS to single-crystal surfaces, its enhancement factor (10^6–10^7) is ultimately limited by the dielectric shell. NCERS overcomes this limitation by creating sub-10 nm metal-metal or metal-dielectric cavities. These nanostructures provide extreme electromagnetic field localization while offering binding sites that effectively capture target molecules. The resulting gap-plasmon mode achieves the enhancement factors of 10^8–10^{11}, enabling routine detection of sub-monolayer intermediates and even single-molecule events. Therefore, it is particularly suitable for *in-situ* studies of complex interfaces in electrocatalysis.

Wright et al. employed a nanoparticle-on-mirror configuration to monitor the behavior of fewer than $[Ni(tpyS)_2]^{2+}$ molecules inside a single NCERS cavity (Figure 4A) [23]. Combined SERS and density functional theory analysis revealed that the initial activation of CO_2 occurs at the ligands rather than the metal, accompanied by Ni-N bond cleavage and water coordination to form $[L_5Ni\text{-}OH_2]^+$. This intermediate subsequently couples with CO_2 under proton-electron transfer to yield CO. Although single-cavity studies provide molecular information, practical catalysts suffer from nanoscale heterogeneity that could be obscured by ensemble averaging. Moreover, the nanoscale heterogeneity may exhibit microscopic differences in structure, composition, and electronic state of catalytic sites, which greatly limit the in-depth understanding of catalytic reaction mechanisms between single particles or single sites. Therefore, if an advanced imaging method can be integrated to achieve high spatiotemporal resolution Raman characterization of a single particle or even a single site, it will be expected to gain a more comprehensive understanding of the structure-activity relationship of catalysts. As illustrated in Figure 4B, Yang et al. addressed this issue by integrating the plasmon resonance enhancement strategy with a high spatiotemporal resolution Raman system, developing an *in-situ* hyperspectral Raman characterization platform with single-nanocavity resolution [24]. Specifically, they constructed Au@Cu nanoreactors with different gap sizes and monitored C-C coupling pathways. By integrating single-particle coupled scattering intensity, Raman signal, and CO onset potential, this study proposed that the overlap degree of double layers (EDL_S) was the key factor determining the selectivity of the eCO_2RR pathway. In Figure 4C, for the gap with a smaller size, the overlap of EDL_S promoted the enrichment of *CO intermediates, thereby preferentially inducing the CO-CO coupling pathway and forming OC**COH (1230 cm^{-1}). In Figure 4D, for the gap with a larger size, the reaction favored the proton-assisted CHO-CO pathway, generating intermediates such as O*CCHO (973 cm^{-1}, 1278 cm^{-1}) and *OCHCHO* (1373 cm^{-1}). Finite-element simulation confirms that smaller gaps shift negatively the compact-layer potential, lowering the CO formation overpotential and accelerating *CO dimerization. By correlating individual cavity geometries with their respective reaction pathways, this work provides a spatially resolved roadmap for catalyst design. Therefore, NCERS improved spatial resolution and achieved single-site sensitivity, offering a powerful complement to SHINERS and regular SERS for probing complex electrochemical interfaces.

3.4. MEA-Based In-Situ Raman Spectroscopy

Recently, the development of Raman spectroscopy techniques has focused on real-time *in-situ* characterization of complex electrode structures under *operando* conditions of high current density, zero-gap structure, and polymer electrolyte interface. However, traditional liquid electrolyte-based Raman techniques suffer from some application limitations under *operando* conditions. For example, high current density not only generates multiple bubbles to physically disturb the electrode/electrolyte interface, but also results in an extremely fast renewal rate of interfacial species, which makes it difficult to capture reaction intermediates in real time. MEA-adapted Raman spectroscopy integrates directly the plasmonic hotspot into the working electrode while employing ultrathin windows or cross-sectional (CS) imaging to maintain optical access. It enables reliable *in-situ* tracking of dynamic evolution and spatial distribution of intermediates in eCO_2RR, and reveals unobservable reaction mechanisms in traditional liquid electrolytes. Additionally, it also combines complementary techniques like MS to achieve synchronous correlation between reaction intermediates and corresponding products.

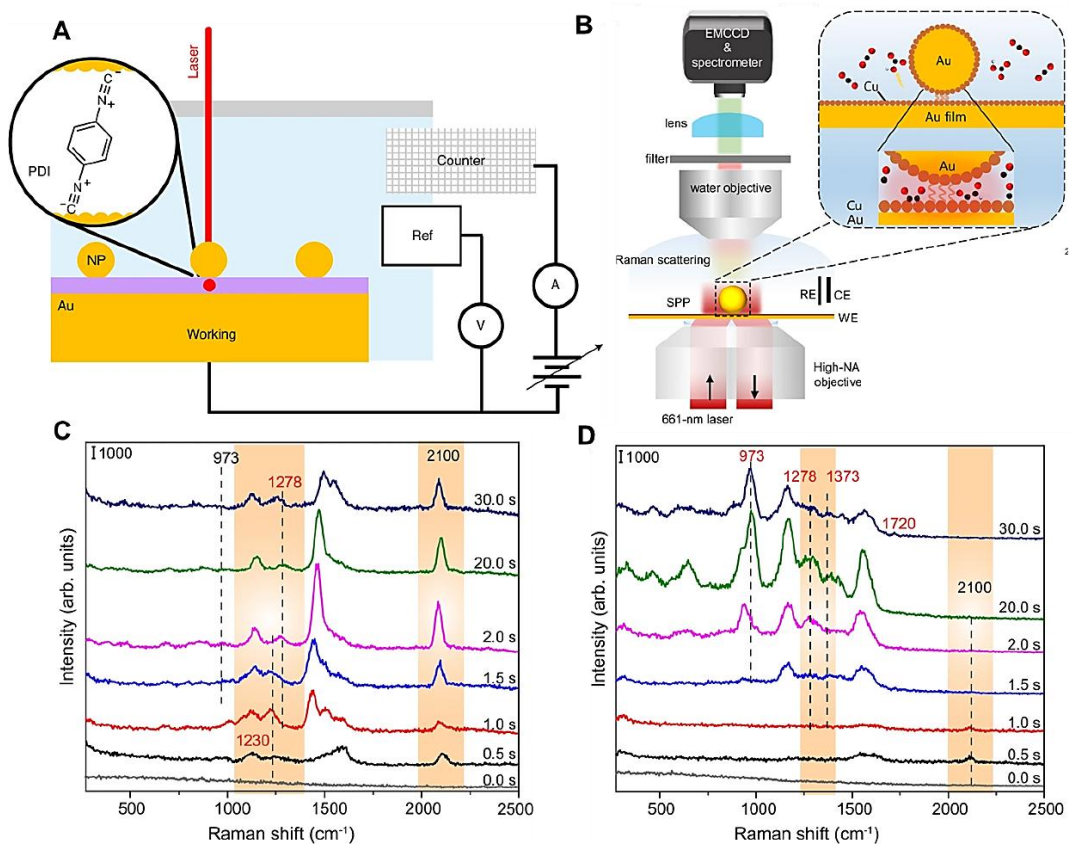

Figure 4. Correlating local electric field effects with reaction pathways at the single-nanocavity level using NCERS. (**A**) Nanoparticle-on-mirror configuration for *operando* tracking of $[Ni(tpyS)_2]^{2+}$ molecular. Adapted from Ref. [23] with permission. Copyright 2021, Springer Nature. (**B**) Schematic illustration of hyperspectral NCERS setup enabling single-nanocavity Raman mapping. Timeseries of Raman spectra at single nanocavities with a smaller gap (**C**) and with a larger gap (**D**) when a potential of −0.6 V (vs. Ag/AgCl) is applied. Adapted from Ref. [24] with permission. Copyright 2024, Springer Nature. NCERS, nanoconfinement-enhanced Raman spectroscopy.

In Figure 5A, Wang et al. constructed an *operando* Raman-MS platform compatible with a pure water-based MEA electrolyser (Figure 5A), first observing *CCO specie as a key intermediate for C_2 products [25]. At 400 mA cm^{-2}, bridge-adsorbed CO (CO_B, 1860 cm^{-1}) dominates the Cu/ionomer interface, whereas the traditionally observed linear-adsorbed CO (CO_L, 2070 cm^{-1}) is almost absent. Subsequently, isotope labelling ($^{13}CO_2$ and D_2O) confirmed the assignment of the Raman band at 360 cm^{-1} to *CCO, that a C_2 intermediate related to C_2H_4 formation (Figure 5B). Notably, the unique environment of MEA electrolyzers with reduced water content and constrained water mobility causes the rate-determining step to shift from C-C coupling to *CCO reduction. Similarly, Xu et al. developed a cross-section (CS) MEA-based Raman spectroscopy to image the spatial distribution of intermediates across the 8-μm-thick catalyst layer under industrial current densities up to 200 mA cm^{-2} (Figure 5C) [26]. They mapped CO_L and CO_B intensities at current densities from 10 to 200 mA cm^{-2} (Figure 5D). CO_L-dominated regions exhibited CO_2RR activity of 2–3 fold higher than CO_B-dominated regions. Furthermore, the CO_L fraction reduced toward the gas-diffusion side as humidity decreased. Under dry CO_2, the active zone is confined to the first 2 μm adjacent to the anion-exchange membrane, whereas elevated humidity or higher current pushes the reaction toward the electrode center. These observations reveal that local reactant availability and electric-field distribution can simultaneously control catalyst utilization inside practical devices. Compared to conventional half-cell conditions, MEA-based Raman systems exhibit distinct characteristics in zero-gap electrolysers, underscoring the necessity of *operando* vibrational spectroscopy for guiding selective CO_2 reduction.

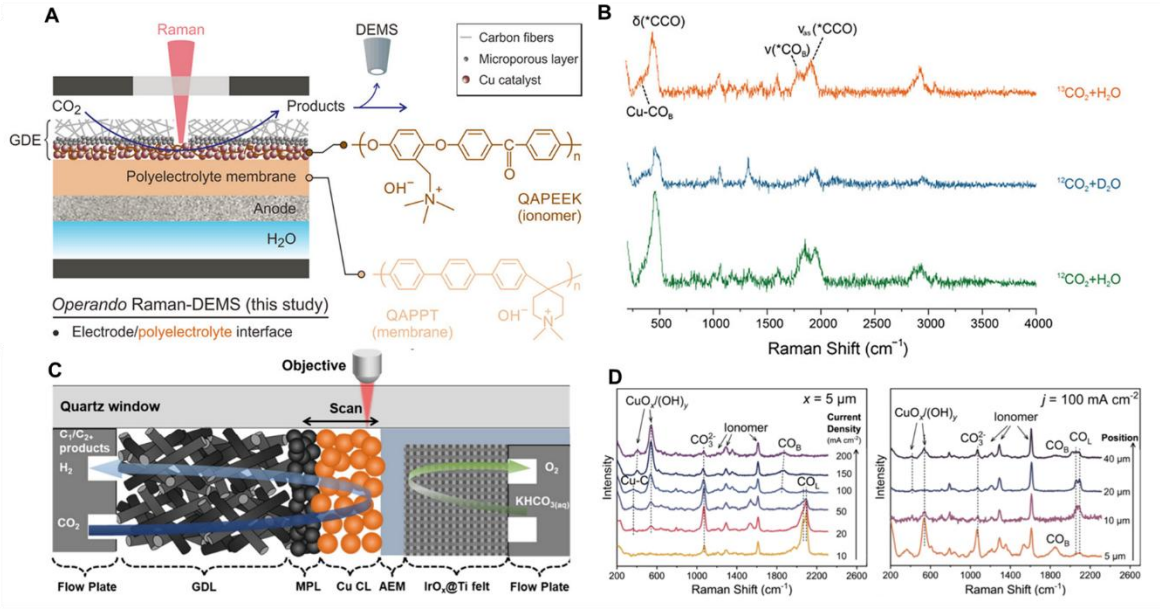

Figure 5. Visualizing spatial distribution of intermediates under *operando* current densities using MEA-based Raman Spectroscopy. (**A**) *Operando* Raman-MS platform for the Cu/ionomer interface in a pure-water MEA. (**B**) Isotope-labelled spectra evidencing *CCO as the C_2 precursor under 400 mA cm^{-2}. Adapted from Ref. [25] with permission. Copyright 2025, Wiley. (**C**) Schematic of an *in-situ* CS-Raman cell. (**D**) *In-situ* CS-Raman spectra on Cu catalyst layer at a fixed position (x = 5 μm) under current densities ranging from 10 to 200 mA cm^{-2} and spatial profiles of CS-Raman spectra at 100 mA cm^{-2} at various positions. Adapted from Ref. [26] with permission. Copyright 2025, American Chemical Society. MEA, membrane electrode assembly; CS, cross-section.

3.5. STR-SERS

The formation and coupling of reaction intermediates, as well as the reconstruction of the catalyst surface, may happen on a timescale near or below one second, depending on reaction conditions. Therefore, *in situ* time-resolved spectroscopic techniques are necessary to improve temporal resolution in order to deeply investigate the reaction kinetics. STR-SERS can track fast interfacial reactions by integrating the high sensitivity of SERS with the dynamic capture capability of sub-second time-resolved techniques [51]. For example, Ruiter et al. employed STR-SERS to conduct real-time tracking of the structural evolution and intermediate transformation on the Cu electrode surface during the eCO_2RR process [27]. By subjecting the Cu electrode to anodic oxidation and reduction treatment, nanostructured hotspots with high SERS activity were constructed *in situ*. Finally, the Raman signals were acquired with a high temporal resolution of 0.7 s. Raman spectra revealed two key CO intermediates. The first was high-frequency linearly adsorbed CO at 2092 cm^{-1}, which was stably adsorbed on isolated defect sites and primarily associated with CO formation. The second was low-frequency linearly adsorbed CO, less than 2060 cm^{-1} that appeared at −0.9 V and exhibited a significant Stark shift, whose dynamic behavior was closely associated with C-C coupling and ethylene formation. This work demonstrated that low-frequency linearly adsorbed CO served as an important precursor of ethylene, and highlighted the importance of future millisecond-scale time-resolved *in-situ* Raman spectroscopy for elucidating eCO_2RR.

4. Raman Cell Innovations

The design of the Raman cell is significantly crucial for improving the practicality of *in-situ*/*operando* Raman spectroscopy techniques. However, conventional complex configurations of *in-situ* Raman spectroscopy often face several challenges, including optical focusing and limited spatial resolution. These issues can lead to signal attenuation and difficulty in capturing transient intermediates. Recent Raman cell innovations have emerged to address these challenges, particularly focusing on the design of flow-cell and gas diffusion electrodes (GDEs) setups [52–54].

Notably, Xu et al designed an *in-situ* spectroscopic electrolyzer that enables direct characterization of the catalyst layer CS via confocal Raman spectroscopy [55]. The CS of the GDE is sealed and pressed on a thin quartz optical window. Through this window, the Raman laser can be focused on different regions of the catalyst layer. The technique successfully distinguished multiple regions within the catalyst layer, which exhibit different morphologies under various reaction conditions. Therefore, this study improves the spatial resolution and directly

reveals the spatial distribution of reactants, intermediates, and products inside the catalyst layer. This advancement enables a more effective capture of key reaction processes and leads to a more accurate mechanistic understanding. Furthermore, the innovations of flow-cell include the use of thin-layer electrochemical cells with optimized window materials to minimize signal attenuation and allow precise laser focusing. Moreover, microfluidic flow-cells integrated with Raman spectroscopy enable real-time monitoring under controlled flow conditions, reducing bubble accumulation and improving signal stability. These developments make Raman spectroscopy more accessible for studying eCO_2RR under realistic conditions.

5. Mechanism Mapping of Raman-Observable Intermediates

To strengthen the mechanism interpretation of eCO_2RR and link specific Raman bands with elementary reaction steps, a schematic mechanism map was presented in Figure 6. It integrated key Raman-active intermediates identified across various *in-situ*/*operando* Raman techniques and correlated them with their respective elementary steps in the CO_2 reduction pathway. This mechanism map provides a unified framework for interpreting Raman spectra in the reaction process. For instance, the *COOH species represents the early-stage proton-coupled electron transfer step for C_1 product formation [56]. The *CO intermediate serves as a branching node, leading either to desorption (CO product) or further C-C coupling [57]. The *OCCO, *COH, and *CHO species are critical for C-C coupling and C_{2+} product generation [58]. By anchoring key Raman-observable intermediates to specific mechanism steps, this schematic facilitates a more intuitive understanding of how Raman spectroscopy decouples complex reaction pathways. Moreover, representative vibrational bands including *COOH, *CO, *COH, *CHO, *OCCO, *CCO, O*CCHO, O*CHCHO, OC**COH were summarized in Table 2 [24,56–59].

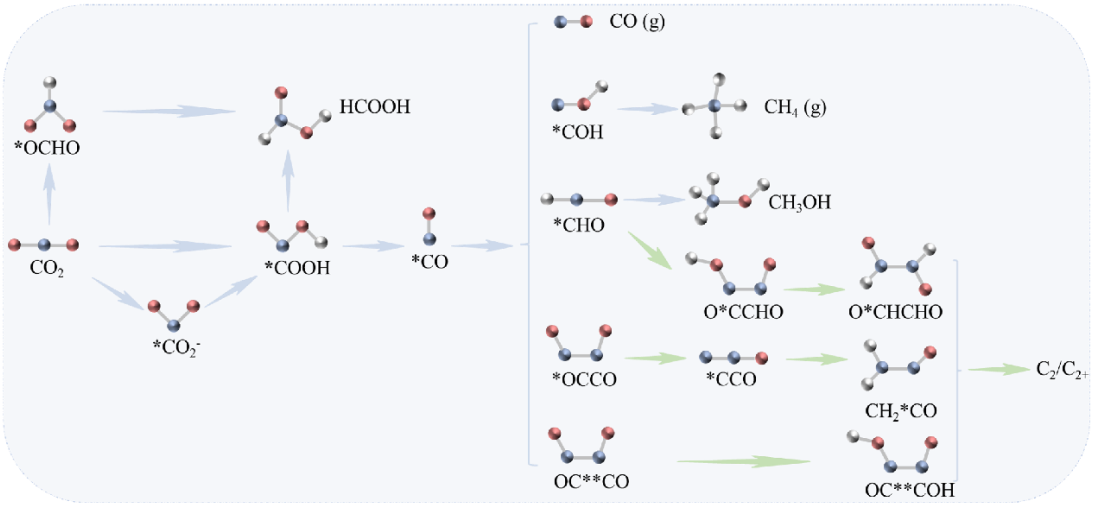

Figure 6. Schematic illustration of Raman-observable intermediates and their corresponding elementary steps in eCO_2RR.

Table 2. Representative Raman bands of key intermediates.

Intermediates	Raman Shifts	Intermediates	Raman Shifts
$*CO_2^-$	1324/1558 cm^{-1}	*OCCO	2088 cm^{-1}
*COOH	1045 cm^{-1}	O*CCHO	973/1278 cm^{-1}
*CO	2030–2070 cm^{-1}	*CCO	460/1945 cm^{-1}
*COH	1305 cm^{-1}	O*CHCHO	1373 cm^{-1}
*CHO	1720 cm^{-1}	OC**COH	1230 cm^{-1}

6. Conclusions and Perspectives

In summary, this minireview has highlighted the pivotal role of advanced *in-situ*/*operando* Raman spectroscopy techniques in decoupling the complex mechanisms of eCO_2RR. By leveraging various enhancement strategies, these techniques have provided new insights into active-phase dynamics, intermediate identification, and reaction pathways under realistic working conditions.

Despite the remarkable progress, several unresolved challenges must be overcome to fully unlock the stronger capacities of these techniques. First, Raman spectroscopy techniques suffer from inherent technical limitations,

including the intrinsically weak signal, which demands boosting sensitivity. Second, due to the effect of factors like spatially heterogeneous electromagnetic enhancement and molecular orientation effects, Raman spectroscopy techniques find it hard to achieve accurate quantification. Besides, establishing a direct quantitative link between the dynamic evolution of active phases with catalytic performance metrics is also exceptionally challenging but essential. Third, spectral complexity often leads to identify ambiguously. The overlap of Raman bands from various surface species and intermediates can obscure their identities, risking misinterpretation. Finally, the spectral interferences from electrolytes, bubbles, and cell windows in *operando* measurement conditions also persist. Therefore, in the future, addressing these challenges requires great efforts towards multimodal integration, advanced data analysis, and instrumental innovation.

6.1. Multimodal Platforms

Future efforts can consider the integration of *in-situ* Raman spectroscopy with complementary techniques such as XAS and infrared spectroscopy within a single experimental setup. XAS can provide simultaneous information on the electronic structure and coordination environment of the metal centers, while infrared spectroscopy offers complementary vibrational information that can help confirm intermediate identities. Such technique coupling would provide a cross-validated, comprehensive view of the reaction interface for precise intermediate assignment and mechanistic elucidation. Moreover, combining with quantitative techniques like MS, *in-situ* Raman spectroscopy is poised to evolve from a powerful qualitative tool into a precise quantitative analytical technique.

6.2. Advanced Analytical Tools

The massive and complex spectral data generated by *in-situ* Raman characterization techniques demand advanced analytical tools. Conventional manual analysis is inadequate for extracting untraceable trends and correlations. The application of machine learning (ML), particularly unsupervised learning for spectral clustering and feature extraction, and supervised learning for building structure-activity relationships, presents a transformative opportunity. ML models can deconvolute overlapping peaks and identify latent intermediate species. Moreover, they are expected to construct a quantitative structure-activity relationship, transforming data into predictive insights, building a quantitative link between the dynamic evolution of active phases with catalytic performance metrics.

6.3. Instrumental Innovation

Future developments must couple with innovations in spectro-electrochemical cell design. This includes creating versatile cells that can adapt to wider reaction conditions to minimize spectral interference from electrolytes, bubbles, and cell windows. Moreover, they are compatible with standardized protocols, ensuring reproducibility and reliability.

By strategic advancements along these directions, *in-situ* Raman spectroscopy will evolve from a primarily descriptive tool into a robust, predictive platform that can provide quantitative descriptors to accelerate the rational design of high-performance eCO_2RR catalysts.

Funding

This work was supported by the National Natural Science Foundation of China (Grant No. 22174061 and 22374072) and State Key Laboratory of Analytical Chemistry for Life Science (Grant No. 5431ZZXM2502).

Data Availability Statement

No data was used for the research described in the article.

Conflicts of Interest

The authors declare no conflict of interest.

Use of AI and AI-Assisted Technologies

No AI tools were utilized for this paper.

References

1. O'Brien, C.P.; Miao, R.K.; Shayesteh Zeraati, A.; et al. CO_2 Electrolyzers. *Chem. Rev.* **2024**, *124*, 3648–3693.
2. Sun, Q.; Jia, C.; Lu, H.; et al. Ampere-Level Electroreduction of CO_2 and CO. *Chem. Soc. Rev.* **2025**, *54*, 6973–7016.
3. Nitopi, S.; Bertheussen, E.; Scott, S.B.; et al. Progress and Perspectives of Electrochemical CO_2 Reduction on Copper in Aqueous Electrolyte. *Chem. Rev.* **2019**, *119*, 7610–7672.
4. Guan, Y.; Li, Y.; Li, Z.; et al. Promotion of C-C Coupling in the CO_2 Electrochemical Reduction to Valuable C_{2+} Products: From Micro-Foundation to Macro-Application. *Adv. Mater.* **2025**, *37*, 2417567.
5. Song, Y.F.; Zhang, X.M.; Xie, K.; et al. High-Temperature CO_2 Electrolysis in Solid Oxide Electrolysis Cells: Developments, Challenges, and Prospects. *Adv. Mater*. **2019**, *31*, 1902033.
6. Firet, N.J.; Smith, W.A. Probing the Reaction Mechanism of CO_2 Electroreduction over Ag Films via *Operando* Infrared Spectroscopy. *ACS Catal.* **2017**, *7*, 606–612.
7. Yao, Z.; Cheng, H.; Xu, Y.; et al. Hydrogen Radical-Boosted Electrocatalytic CO_2 Reduction Using Ni-Partnered Heteroatomic Pairs. *Nat. Commun.* **2024**, *15*, 9881.
8. Lim, C.Y.J.; Yilmaz, M.; Arce-Ramos, J.M.; et al. Surface Charge as Activity Descriptors for Electrochemical CO_2 Reduction to Multi-Carbon Products on Organic-Functionalised Cu. *Nat. Commun*. **2023**, *14*, 335.
9. Liu, H.M.; Yan, T.; Tan, S.D.; et al. Observation on Microenvironment Changes of Dynamic Catalysts in Acidic CO_2 Reduction. *J. Am. Chem. Soc*. **2024**, *146*, 5333–5342.
10. Zhang, W.; Yu, A.; Mao, H.Y.; et al. Dynamic Bubbling Balanced Proactive CO_2 Capture and Reduction on a Triple-Phase Interface Nanoporous Electrocatalyst. *J. Am. Chem. Soc*. **2024**, *146*, 21335–21347.
11. Hsu, C.S.; Wang, J.; Chu, Y.C.; et al. Activating Dynamic Atomic Configuration for Single-Site Electrocatalyst in Electrochemical CO_2 Reduction. *Nat. Commun.* **2023**, *14*, 5245.
12. Phong Duong, H.; Rivera de la Cruz, J.G.; Portehault, D.; et al. Incorporation of Isolated Ag Atoms and Au Nanoparticles in Copper Nitride for Selective CO Electroreduction to Multicarbon Alcohols. *Nat. Mater.* **2025**, *24*, 900–906.
13. Wang, M.; Li, Y.; Jia, J.; et al. Tuning Catalyst-Support Interactions Enable Steering of Electrochemical CO_2 Reduction Pathways. *Sci. Adv.* **2025**, *11*, eado5000.
14. Zang, Y.; Wang, S.; Sang, J.; et al. Illustration of the Intrinsic Mechanism of Reconstructed Cu Clusters for Enhanced CO_2 Electroreduction to Ethanol Production with Industrial Current Density. *Nano Lett.* **2024**, *24*, 7261–7268.
15. Hou, J.; Chang, X.; Li, J.; et al. Correlating CO Coverage and CO Electroreduction on Cu via High-Pressure *in Situ* Spectroscopic and Reactivity Investigations. *J. Am. Chem. Soc.* **2022**, *144*, 22202–22211.
16. Gao, W.; Xu, Y.; Fu, L.; et al. Experimental Evidence of Distinct Sites for CO_2-to-CO and CO Conversion on Cu in the Electrochemical CO_2 Reduction Reaction. *Nat. Catal.* **2023**, *6*, 885–894.
17. Luo, Y.; Sheng, S.; Pisarra, M.; et al. Selective excitation of vibrations in a single molecule. *Nat. Commun.* **2024**, *15*, 6983.
18. Li, J.; Chen, G.X.; Zhu, Y.Y.; et al. Efficient Electrocatalytic CO_2 Reduction on a Three-Phase Interface. *Nat. Catal*. **2018**, *1*, 592–600.
19. Zhang, D.; Liu, X.; Zhao, Y.; et al. *In situ* Raman Spectroscopic Studies of CO_2 Reduction Reactions: From Catalyst Surface Structures to Reaction Mechanisms. *Chem. Sci.* **2025**, *16*, 4916–4936.
20. Pérez-Jiménez, A.I.; Lyu, D.; Lu, Z.X.; et al. Surface-Enhanced Raman Spectroscopy: Benefits, Trade-Offs and Future Developments. *Chem. Sci*. **2020**, *11*, 4563–4577.
21. Zhao, Y.; Chang, X.; Malkani, A.S.; et al. Speciation of Cu Surfaces During the Electrochemical CO Reduction Reaction. *J. Am. Chem. Soc.* **2020**, *142*, 9735–9743.
22. Zhao, Y.; Zhang, X.G.; Bodappa, N.; et al. Elucidating Electrochemical CO_2 Reduction Reaction Processes on Cu(hkl) Single-Crystal Surfaces by *in Situ* Raman Spectroscopy. *Energy Environ. Sci.* **2022**, *15*, 3968–3977.
23. Wright, D.; Lin, Q.; Berta, D.; et al. Mechanistic Study of an Immobilized Molecular Electrocatalyst by *in Situ* Gap-Plasmon-Assisted Spectro-Electrochemistry. *Nat. Catal.* **2021**, *4*, 157–163.
24. Yang, R.; Cai, Y.; Qi, Y.; et al. How Local Electric Field Regulates C-C Coupling at a Single Nanocavity in Electrocatalytic CO_2 Reduction. *Nat. Commun.* **2024**, *15*, 7140.
25. Wang, J.; Huang, B.; Xiao, L.; et al. *Operando* Spectroscopic Insights into CO_2 Reduction at Electrode/Polyelectrolyte Interfaces. *Angew. Chem. Int. Ed.* **2025**, *64*, e202509423.
26. Fu, L.; He, P.; Wu, C.; et al. Distribution of Speciation and Activity Across the Catalyst Layer during CO_2 Electroreduction in Membrane Electrode Assembly. *ACS Energy Lett.* **2025**, *10*, 3445–3450.
27. An, H.; Wu, L.; Mandemaker, L.D.B.; et al. Sub-Second Time-Resolved Surface-Enhanced Raman Spectroscopy Reveals Dynamic CO Intermediates during Electrochemical CO_2 Reduction on Copper. *Angew. Chem. Int. Ed.* **2021**, *60*, 16576–16584.
28. Chen, H.Q.; Zou, L.; Wei, D.Y.; et al. *In Situ* Studies of Energy-Related Electrochemical Reactions Using Raman and X-

Ray Absorption Spectroscopy. *Chin. J. Catal.* **2022**, *43*, 33–46.
29. He, Q.F.; Zhang, Y.J.; Yang, Z.L.; et al. Surface-Enhanced Raman Spectroscopy: Principles, Methods, and Applications in Energy Systems. *Chin. J. Chem.* **2023**, *41*, 355–369.
30. He, Q.F.; Yu, J.; Dong, J.C.; et al. Recent Advances in Raman Spectroelectrochemistry on Single-Crystal Surfaces. *Sci. China Chem.* **2023**, *66*, 3360–3371.
31. Song, J.T.; Qian, Z.X.; Yang, J.; et al. *In Situ/Operando* Investigation for Heterogeneous Electro-Catalysts: From Model Catalysts to State-of-the-Art Catalysts. *ACS Energy Lett.* **2024**, *9*, 4414–4440.
32. Zhu, Y.Z.; Zhou, R.Y.; Hu, S.; et al. Shell-Isolated Nanoparticle-Enhanced Raman Spectroscopy: Toward High Sensitivity and Broad Applicability. *ACS Nano*, **2024**, *18*, 32287–32298.
33. Wang, Y.H.; Zheng, S.; Yang, W.M.; et al. *In Situ* Raman Spectroscopy Reveals the Structure and Dissociation of Interfacial Water. *Nature* **2021**, *600*, 81–85.
34. Bao, H.M.; Motobayashi, K.; Zhang, H.W.; et al. *In Situ* Surface-Enhanced Raman Spectroscopy Reveals a Mars-van Krevelen-Type Gas Sensing Mechanism in Au@SnO_2 Nanoparticle-Based Chemiresistors. *J. Phys. Chem. Lett*. **2023**, *14*, 4113–4118.
35. Ze, H.J.; Chen, X.; Wang, X.T.; et al. Molecular Insight of the Critical Role of Ni in Pt-Based Nanocatalysts for Improving the Oxygen Reduction Reaction Probed Using an *in Situ* SERS Borrowing Strategy. *J. Am. Chem. Soc*. **2021**, *143*, 1318–1322.
36. Li, J.F.; Zhang, Y.J.; Ding, S.Y.; et al. Core-Shell Nanoparticle-Enhanced Raman Spectroscopy. *Chem. Rev*. **2017**, *117*, 5002–5069.
37. Chen, M.; Liu, D.; Du, X.; et al. 2D Materials: Excellent Substrates for Surface-Enhanced Raman Scattering in Chemical Sensing and Biosensing. *TrAC-Trend Anal. Chem*. **2020**, *130*, 115983.
38. Wang, X.; Huang, S.C.; Hu, S.; et al. Fundamental Understanding and Applications of Plasmon-Enhanced Raman Spectroscopy. *Nat. Rev. Phys*. **2020**, *2*, 253–271.
39. Yang, P.P.; Zhang, X.L.; Gao, F.Y.; et al. Protecting Copper Oxidation State via Intermediate Confinement for Selective CO_2 Electroreduction to C_{2+} Fuels. *J. Am. Chem. Soc*. **2020**, *142*, 6400–6408.
40. Yang, F.; Jiang, S.; Liu, S.; et al. Dynamics of Bulk and Surface Oxide Evolution in Copper Foams for Electrochemical CO_2 Reduction. *Commun. Chem*. **2024**, *7*, 66.
41. Li, J.F.; Huang, Y.F.; Ding, Y.; et al. Shell-Isolated Nanoparticle-Enhanced Raman Spectroscopy. *Nature* **2010**, *464*, 392–395.
42. Hansen, K.U.; Cherniack, L.H.; Jiao, F. Voltage Loss Diagnosis in CO_2 Electrolyzers Using Five-Electrode Technique. *ACS Energy Lett.* **2022**, *7*, 4504–4511.
43. Chen, C.; Li, Y.; Yang, P. Address the "Alkalinity Problem" in CO_2 Electrolysis with Catalyst Design and Translation. *Joule* **2021**, *5*, 737–742.
44. Mi, Z.; Wang, T.; Xiao, L.; et al. Catalytic Peculiarity of Alkali Metal Cation-Free Electrode/Polyelectrolyte Interfaces Toward CO_2 Reduction. *J. Am. Chem. Soc.* **2024**, *146*, 17377–17383.
45. Hartman, T.; Geitenbeek, R.G.; Wondergem, C.S.; et al. Operando Nanoscale Sensors in Catalysis: All Eyes on Catalyst Particles. *ACS Nano* **2020**, *14*, 3725–3735.
46. Dong, J.C.; Zhang, X.G.; Briega-Martos, V.; et al. *In Situ* Raman Spectroscopic Evidence for Oxygen Reduction Reaction Intermediates at Platinum Single-Crystal Surfaces. *Nat. Energy* **2019**, *4*, 60–67.
47. Yang, S.Y.; Jiang, M.H.; Zhang, W.J.; et al. *In Situ* Structure Refactoring of Bismuth Nanoowers for Highly Selective Electrochemical Reduction of CO_2 to Formate, *Adv. Funct. Mater.* **2023**, *33*, 2301984.
48. Handoko, A.D.; Wei, F.; Jenndy; et al. Understanding Heterogeneous Electrocatalytic Carbon Dioxide Reduction through *Operando* Techniques. *Nat. Catal.* **2018**, *1*, 922–934.
49. Zhang, H.; Wang, C.; Sun, H.L.; et al. *In Situ* Dynamic Tracking of Heterogeneous Nanocatalytic Processes by Shell-Isolated Nanoparticle-Enhanced Raman Spectroscopy. *Nat. Commun*. **2017**, *8*, 15447.
50. You, X.Q.; Zhang, D.A.; Zhang, X.G.; et al. Exploring the Cation Regulation Mechanism for Interfacial Water Involved in the Hydrogen Evolution Reaction by *in Situ* Raman Spectroscopy. *Nano-Micro Lett*. **2024**, *16*, 53.
51. Gunathunge, C.M.; Ovalle, V.J.; Li, Y.; et al. Existence of an Electrochemically Inert CO Population on Cu Electrodes in Alkaline pH. *ACS Catal.* **2018**, *8*, 7507–7516.
52. Lees, E.W.; Mowbray, B.A.W.; Parlane, F.G.L.; et al. Gas Diffusion Electrodes and Membranes for CO_2 Reduction Electrolysers. *Nat. Rev. Mater.* **2022**, *7*, 55–64.
53. Tan, X.; Sun, K.; Zhuang, Z.; et al. Stabilizing Copper by a Reconstruction-Resistant Atomic Cu-O-Si Interface for Electrochemical CO_2 Reduction. *J. Am. Chem. Soc.* **2023**, *145*, 8656–8664.
54. Kibria, M.G.; Edwards, J.P.; Gabardo, C.M.; et al. Electrochemical CO_2 Reduction into Chemical Feedstocks: From Mechanistic Electrocatalysis Models to System Design. *Adv. Mater.* **2019**, *31*, 1807166.
55. Sun, Q.; Wang, J.; Fu, L.; et al. Probing Inside the Catalyst Layer on Gas Diffusion Electrodes in Electrochemical

Reduction of CO and CO_2. *Angew. Chem. Int. Ed.* **2025**, *64*, e202504715.
56. Chernyshova, I.V.; Somasundaran, P.; Ponnurangam, S. On the Origin of the Elusive First Intermediate of CO_2 Electroreduction. *Proc. Natl. Acad. Sci. USA* **2018**, *115*, E9261–E9270.
57. Bohra, D.; Ledezma-Yanez, I.; Li, G.; et al. Lateral Adsorbate Interactions Inhibit HCOO@ while Promoting CO Selectivity for CO_2 Electrocatalysis on Silver. *Angew. Chem. Int. Ed.* **2019**, *58*, 1520–1520.
58. Zhan, C.; Dattila, F.; Rettenmaier, C.; et al. Key Intermediates and Cu Active Sites for CO_2 Electroreduction to Ethylene and Ethanol. *Nature Energy*, **2024**, *9*, 1485–1496.
59. Xie, Y.; Ou, P.; Wang, X.; et al. High Carbon Utilization in CO_2 Reduction to Multi-Carbon Products in Acidic Media. *Nat. Catal.* **2022**, *5*, 564–570.